International Journal of Thermal Sciences 48 (2009) 1960–1966

Contents lists available at ScienceDirect

International Journal of Thermal Sciences

journal homepage: www.elsevier.com/locate/ijts

Laser consecutive pulse heating and phase change: Influence of spatial distribution of laser pulse intensity on melting

S.Z. Shuja, B.S. Yilbas*, Shafique M.A. Khan

ME Department, King Fahd University of Petroleum and Minerals, KFUPM Box 1913, Dhahran 31261, Saudi Arabia

ARTICLE INFO

Article history:
Received 28 October 2008
Received in revised form
28 February 2009
Accepted 28 February 2009
Available online 26 March 2009

Keywords:
Laser
Consecutive pulse
Heating
Phase change

ABSTRACT

Laser consecutive pulse heating of solid surface and the influence of the laser pulse parameter on the melting and mushy zone formation in the irradiated region are investigated. The laser pulse parameter (β) defines the spatial distribution of the laser pulse power at the irradiated surface; in which case, $\beta = 0$ represents the Gaussian profile while $\beta = 1$ corresponds to the ring type of laser power distribution with the peak intensity away from the center (symmetry axis). β is set in such a way that the energy content in each pulse with different β values becomes the same. The control volume approach is used when modeling the heating and phase change processes. The laser pulse parameter is selected to alter the laser power intensity distribution across the irradiated surface while modifying the location and magnitude of the laser peak power intensity at the irradiated surface. It is found that the laser pulse parameter alters the sizes of the melting and mushy zones in the surface region.

1. Introduction

Laser heat treatment of metallic surfaces finds application in manufacturing industry, which is because of the localized and precise heating situations. The high power laser beam when focused onto the solid surface, solid heating and subsequent phase change process takes place at the irradiated surface. This process can alter the composition of the substrate material and changes the metallurgical structure in the irradiated region due to high cooling rates resulted in the cooling cycle. In the surface treatment applications, the laser output power is either in continuous (cw) or in consecutive pulses (pulse repetition) forms. In the application of consecutive pulses, controlled melting in the irradiated region can be possible through adjusting the duty cycle of the consecutive pulses and altering the intensity distribution across the irradiated spot. Moreover, the model studies provide information on the physical process taking place during the laser irradiation. Consequently, investigation into the effects of the pulse duty cycle and radial distribution of the laser beam intensity at the surface on the laser melting process becomes essential.

Considerable research studies were carried out to examine the laser heating and phase change processes. The transport phenomena and keyhole dynamics during pulsed laser welding was investigated by Zhou et al. [1]. They accommodated the Marangoni shear force when modeling the keyhole formation and indicated that predictions of weld depth agreed with the experimental findings. The numerical analysis of the effects of non-conventional laser beam geometries in relation to laser melting of metallic materials was studied by Safdar et al. [2]. They predicted temperature distribution and melt size in the irradiated region after considering the surface heat source model. Zhou et al. [3] investigated the heat transfer, fluid flow, and keyhole dynamics during a pulsed laser melting process. They used the enthalpy method to account for the phase change in the laser irradiated region. The nano-scale machining using the electron and laser beam was investigated by Wong et al. [4]. They used a Monte Carlo approach and Fresnel reflections to simulate laser heating process. The momentum, heat and mass transfer analysis in laser surface alloying were carried out by Raj et al. [5]. They employed particle-tracking algorithm and a simultaneous particle melting consideration in the numerical simulations. A mathematical model for laser powder deposition and prediction of the melt pool depth and dilution was presented by Fathi et al. [6]. They showed that the melt pool depth was the maximum at a certain process speed. An analytical model for laser heating and melting was presented by Shen et al. [7]. They indicated that discontinuity in the temperature gradient was obvious due to the latent heat of fusion and the increment in thermal conductivity in the solid phase. Van de Ven and Erdman [8] investigated the laser transmission welding of thermoplastics. They developed a mathematical model to simulate

* Corresponding author. Tel.: +966 38604481; fax: +966 38602949.
E-mail address: bsyilbas@kfupm.edu.sa (B.S. Yilbas).

1290-0729/$ – see front matter © 2009 Elsevier Masson SAS. All rights reserved.
doi:10.1016/j.ijthermalsci.2009.02.022

Nomenclature

a	Gaussian parameter (m)
A_{mush}	mushy zone constant
c_p	specific heat capacity (J/kg K)
H	total enthalpy (J/K)
h	enthalpy (J/kg K)
h_{ref}	reference enthalpy (J/kg K)
h_t	heat transfer coefficient (W/m^2 K)
I_o	laser peak power intensity (W/m^2)
k	thermal conductivity (W/m K)
T	temperature (°C)
$T_{liquidus}$	liquid temperature (°C)
$T_{solidus}$	solid temperature (°C)
t_c	end of cooling period (s)
t_f	beginning of falling period of the consecutive pulse(s)
t_p	pulse length of the consecutive pulse (s)
t_r	end of rise period of the consecutive pulse (s)
r	radial distance (m)
r_f	reflection coefficient
S	momentum sink per unit mass flow rate (m/s)
S_o	source term (W/m^3)
T_o	initial temperature (°C)
t	time (s)
v	velocity (m/s)
z	axial distance (m)

Greek symbols

β	laser pulse parameter
γ	the liquid fraction
ε	porosity
ρ	density (kg/m^3)
$\alpha(=\frac{k}{\rho c_{p_s}})$	thermal diffusivity (m^2/s)
δ	absorption depth (m^{-1})

the laser transmission welding process through which temperature was predicted in the welding section. The enthalpy based lattice Boltzmann model for dominated solid–liquid phase transformation was introduced by Chatterjee and Chakraborty [9]. They modified the latent heat updating procedure to integrate with the lattice Boltzmann equation predicting the liquid fraction during the continuous evolution of the solid–liquid interface. Thermal behavior and melt pool model in laser material processing were investigated by Sarkar et al. [10]. They model the phase change process using a fixed grid enthalpy–porosity technique, which was capable of predicting continuous evolving solid–liquid interface. Laser heating and phase change in the irradiated region was examined by Yilbas and Ben Mansoor [11] and Yilbas et al. [12]. The model studies provided useful information on the phase change process and cavity formation. However, the analysis was limited with the nanosecond laser pulses and cannot be applicable for millisecond laser pulses, which are often used in practical surface hardening processes [13]. Consequently, further investigation of laser heating and phase change processes for the millisecond laser pulses becomes necessary. Moreover, in laser practical applications, laser heating source consists of consecutive pulses with almost identical intensities and pulse lengths, which need to be accounted in the analysis. In laser surface treatment process, the type of the focusing lens and the focus setting of the lens are important factors to achieve the required size of the melt layer. The Gaussian distribution of the laser power intensity at the irradiated surface results in a melt layer with evaporation at the surface, which enhances the roughness of the resulting surface and limits the practical applications. This situation can be avoided via altering the laser power intensity distribution at the surface; in which case, the peak power intensity can be moved away from the irradiated spot center. Moreover, the special aberration of the lens and defocusing of the focal setting alter the laser power intensity distribution at the irradiated surface. Consequently, investigation into the influence of laser power intensity distribution on the melt size becomes essential.

In the present study, laser consecutive pulse heating of steel surface is considered. The phase change including melting is modeled using the enthalpy method. The influence of laser pulse parameter (β), which modifies the laser pulse intensity distribution at the irradiated surface, on the melting process is examined. It should be noted that $\beta = 0$ is the Gaussian power intensity distribution and $\beta = 1$ is a ring type power intensity distribution with the peak intensity away from the irradiated spot center (symmetry axis). A numerical method employing a control volume approach is introduced to predict temperature field in the liquid and mushy zones as well as in the solid phase.

2. Mathematical modeling

Laser heating situation is shown in Fig. 1. The enthalpy–porosity technique is used to model the melting/solidification process. In this case, the melt interface is tracked through a quantity, which is the liquid fraction. It is the fraction of the cell volume, which is in liquid state to total volume of the concerned cell, which is computed at each iteration through satisfying the enthalpy balance. The mushy zone is a region in which the liquid fraction varies in between 0 and 1. The mushy zone can be modeled as a "pseudo" porous medium, in which the porosity changes from 1 to 0 as the material solidify. Upon fully solidification of the material, the porosity becomes zero in a cell and the fluid velocity drops to zero [14].

2.1. Energy equation

The energy balance in the substrate material can be presented through the enthalpy balance. The enthalpy of the material is computed as the sum of the sensible enthalpy, h, and the fraction of the latent heat of fusion, ΔL ($\Delta L = \gamma L$, where L is the latent heat of fusion), in case if the material undergoes melting:

$$H = h + \Delta L \tag{1}$$

where

$$h = h_{ref} + \int_{T_{ref}}^{T} c_p \mathrm{d}T \tag{2}$$

and h_{ref} = reference enthalpy; T_{ref} = reference temperature; c_p = specific heat at constant pressure.

The liquid fraction, γ, can be defined as:

$$\gamma = 0 \quad if\ T < T_{solidus}$$

$$\gamma = 1 \quad if\ T > T_{liquidus}$$

$$\gamma = \frac{T - T_{solidus}}{T_{liquidus} - T_{solidus}} \quad if\ T_{solidus} < T < T_{liquidus} \tag{3}$$

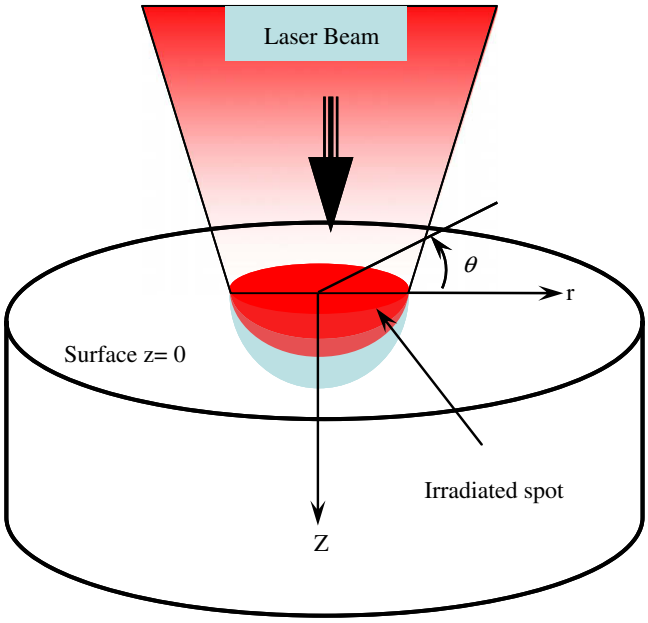

Fig. 1. A schematic view of laser heating situation.

Equation (3) is referred to as the lever rule [14]. The latent heat content can vary between zero (for a solid) and L (for a liquid).

For solidification/melting problems, the energy equation is written as:

$$\frac{\partial}{\partial t}(\rho H) + \nabla\cdot(\rho\vec{v}H) = \nabla\cdot(k\nabla T) + S_o \tag{4}$$

where H is the total enthalpy, ρ is the density, $\vec{v}$ is the fluid velocity, and S_o is the source term.

The volumetric heat source can be arranged to resemble the laser repetitive pulses, i.e.,

$$S_o = I_o\delta\left(1-r_f\right)\exp(-\delta z)\exp\left(-\left(\frac{r}{a}+\beta\right)^2\right)f(t) \tag{5}$$

where I_o, δ, r_f, β, a are the laser peak power intensity, absorption coefficient, reflectivity, laser pulse parameter, the Gaussian beam parameter, and the temporal distribution of laser pulse intensity, respectively. However, the laser pulse energy is kept constant for all the values of the laser pulse parameters considered in the simulations. $\beta = 0$ represents the Gaussian beam profile at the workpiece surface. The temporal variation of the laser pulse shape resembles almost the actual laser pulse shape used in the industry [13], which is in trapezium shape in time domain. The laser pulse parameters used in the simulations are given in Table 1 while Fig. 2 shows the temporal variation of consecutive laser pulses. The time function ($f(t)$) representing the consecutive pulses is:

Table 1
Laser pulse parameters used in the simulations.

Laser pulse parameter (β)	Laser pulse length, t_p (ms)	Cooling period, t_c (ms)	Pulse rise time, t_r (ms)	Pulse fall time, t_f (ms)	Pulse intensity (W/m^2) $\times 10^9$	Gaussian parameter, a (m) $\times 10^{-4}$
Duty cycle 50%	0.05	0.05	0.0065	0.00325	1	2.997

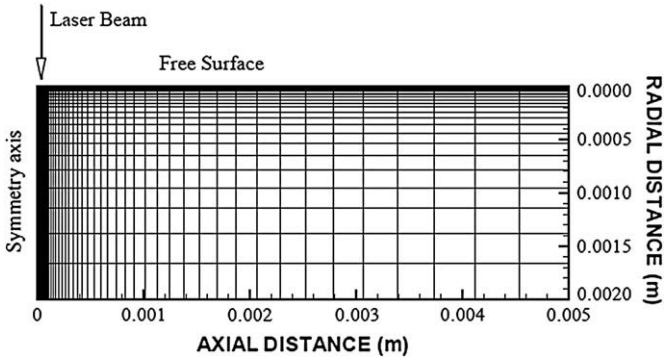

Fig. 2. Grid used in the simulations. The darker lines along the symmetry axis and in the surface region are due to the large number of grid points used in these regions.

$$f(t) = \left\{\begin{array}{ll} 0, & t = 0 \\ 1, & t_r \le t \le \left(t_p - t_f\right) \\ 0, & t = t_p \\ 0, & t_p \le t \le t_c \end{array}\right\} \tag{6}$$

where t_r is the pulse rise time, t_f is the pulse fall time, t_p is the pulse length, t_c is the end of cooling period. $f(t)$ repeats when the second consecutive pulse begins, provided that time $t = t_f + t_c$ corresponds to the starting time of the second pulse. The same mathematical arguments can apply for the other consecutive pulses after the second pulse. In the simulations, 50 consecutive pulses are used, which provides the sufficient liquid layer depth to examine the phase change process in the laser irradiated region.

Since the heating problem is transient, the initial condition should be defined. In this case, initially it is assumed that the slab is at a uniform enthalpy, which can be specified as:

$$At\ t = 0 : T = T_o$$

In order to solve equation (4), two boundary conditions for each principal axis should be specified. The convective boundary is assumed at the surface and radiation heat transfer from the surface is neglected due to a short duration of the laser pulse (0.1 ms), and at a distance considerably away from the surface (at infinity) it is assumed that the heating has no effect on the temperature of the slab; consequently, at a depth of infinity, the temperature is assumed to be constant and equal to the initial temperature of the substrate material. The boundary conditions become:

$$z\ at\ infinity \Rightarrow z = \infty : T(r,\infty,t) = T_o(specified)$$

$$r\ at\ infinity \Rightarrow r = \infty : T(\infty,z,t) = T_o(specified)$$

$$At\ symmetry\ axis \Rightarrow r = 0 : \frac{\partial T(0,z,t)}{\partial r} = 0$$

$$At\ the\ surface \Rightarrow z = 0 : k\frac{\partial T(r,0,t)}{\partial z} = h_t(T_s - T_\infty)$$

where h is the heat transfer coefficient t at the free surface. The heat transfer coefficient predicted earlier [15] is used in the present simulations ($h_t = 10^4$ W/m^2 K). $z = \infty$ and $r = \infty$ are selected such that the boundary conditions do not affect the temperature distribution in the irradiated region as numerically tested, i.e. $z = 2$ mm (thickness of the workpiece) and $r = 5$ mm, which is 16 times the laser beam diameter at the irradiated spot, are selected.

2.2. Momentum equations

The enthalpy–porosity technique deals with the mushy zone (partially solidified region) as a porous medium. The porosity in each cell is set equal to the liquid fraction in that cell. In fully solidified regions, the porosity is equal to zero, which extinguishes the velocities in these regions. The momentum sink due to the reduced porosity in the mushy zone takes the following form [14]:

$$S = \frac{(1-\gamma)^2}{(\gamma^3+\varepsilon)} A_{mush}(\bar{v}) \tag{7}$$

where γ is the liquid volume fraction, ε is a small number (0.001) to prevent division by zero, A_{mush} is the mushy zone constant. The mushy zone constant measures the amplitude of the damping; the higher this value, the steeper the transition of the velocity of the material to zero as it solidifies. The liquid velocity can be found from the average velocity is determined from [14]:

$$\overrightarrow{v_{liq}} = \frac{\overrightarrow{v}}{\gamma} \tag{8}$$

3. Numerical solution

The solution for temperature is essentially iteration between the energy equation (Equation (4)) and the liquid fraction equation (Equation (3)). Directly using Equation (3) to update the liquid fraction usually results in poor convergence of the energy equation; therefore, the method suggested by Voller and Prakash [16] is used to update the liquid fraction based on the specific heat. To discretise the governing equation, a control volume approach is introduced. The details of the numerical scheme are given in [17]. The calculation domain is divided into grids and a grid independence test is performed for different grid sizes and orientation. A non-uniform grid with 350×450 mesh points along z and r axes, respectively, is employed after securing the grid independence. The finer grids are located near the irradiated spot center in the vicinity of the surface and grids become courser as the distance increases towards the bulk of substrate material (Fig. 2). The central difference scheme is adopted for the diffusion terms. A numerical code FLUENT is used to simulate the heating situation. The convergence criterion for the residuals is set as $|\psi^k - \psi^{k-1}| \leq 10^{-6}$ to terminate the simulations; consequently, the converged results are obtained and presented. Table 2 gives the thermal properties of material used in the simulations.

4. Results and discussion

Laser induced phase change in the irradiated region of steel is considered and the effect of pulse profile on the resulting temperature profile and the melt size is examined.

Fig. 3 shows temperature contours for different pulse parameter (β). It should be noted that $\beta = 0$ corresponds to the Gaussian power intensity distribution. This can be observed from Fig. 4; in which, the normalized laser power intensity distribution is shown for different β values. It is evident that energy input during each pulse of consecutive pulses results in extension of high temperature region further into the substrate material, which is particularly true in the radial direction. However, the latent heat of melting beyond the melting temperature suppresses the extension of high temperature region into the substrate material. In this case, energy absorbed from the irradiated field is dissipated through the melting in the irradiated region rather than internal energy gain giving rise to a temperature rise. Moreover, the differences in temperature contours before and after the heating pulse become small in the region close to the mushy zone. This is because of the large size of melting region, in which case, absorption of the incident laser beam takes place in the melting zone and energy transfer from melting region to the solid phase of the substrate is governed by the temperature gradient in this region. Since the irradiated energy is absorbed in the liquid zone, temperature gradients become large within this zone. In this case, temperature gradient remains almost the same in the liquid region close to the mushy zone due to constant temperature constraint across the melting and the mushy zones. Therefore, heat diffusion from the mushy zone to the solid phase almost remains the same during the short duration of

Table 2
Material properties used in the simulations [18,19].

Temp (K)	300	400	600	800	1000	1200	1500
C_p (J/kg K)	477	515	557	582	611	640	682
K (W/m K)	14.9	16.6	19.8	22.6	25.4	28	31.7
ρ (kg/m^3)	8018	7968	7868	7769	7668	7568	7418
L (J/kg)							6258154
T_{solidus} (°C)							1400
T_{liquidus} (°C)							1454
δ (1/m)							6.16×10^7

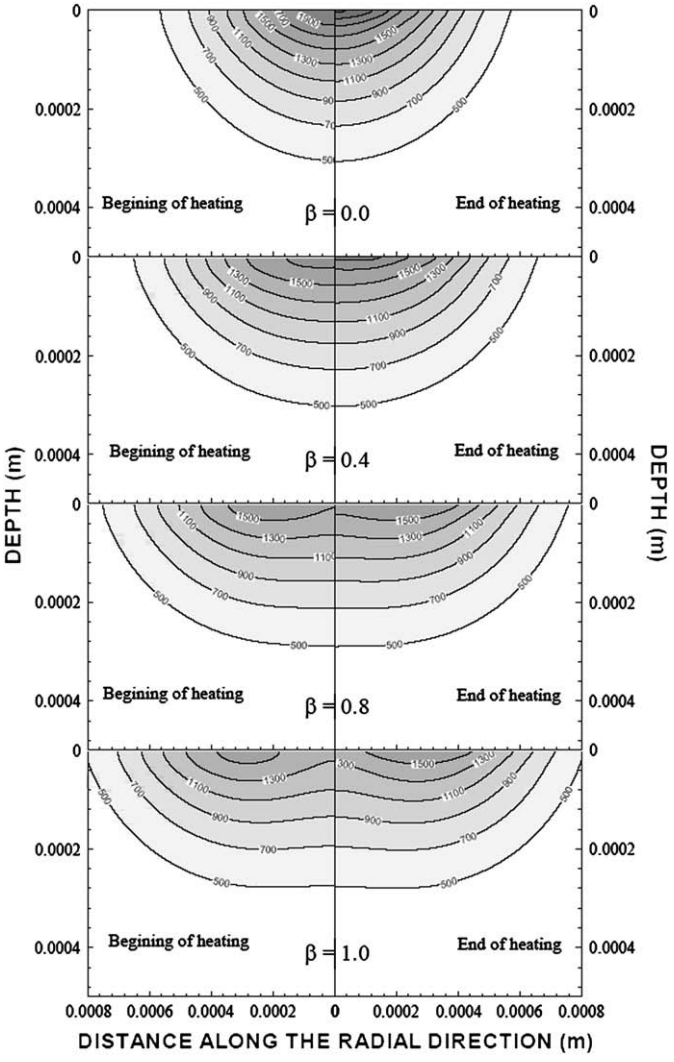

Fig. 3. Temperature contours inside the substrate material for different β.

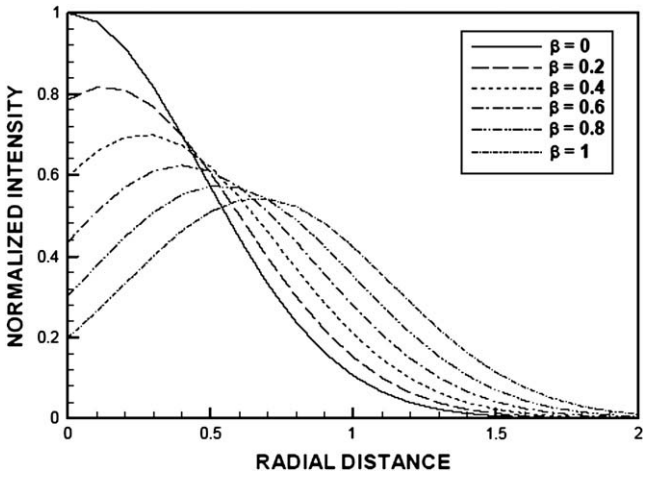

Fig. 4. Spatial distribution of normalized laser pulse intensity along the dimensionless radial distance for different laser pulse parameter (β). The intensity is normalized with the peak intensity for $\beta = 0$ while dimensionless radial distance 2 corresponds to the twice of the laser beam radius.

a single pulse of the consecutive pulses. This results in temperature distribution in the solid phase almost the same. The influence of laser pulse parameter (β) on the temperature profile is significant; in which case, increasing "β" changes the location of the peak power intensity away from the symmetry axis. This lowers temperature rise and size of the melting zone in the vicinity of the symmetry axis.

Fig. 5 shows the liquid and mushy zones in the irradiated region before and after the ending of 50th pulse for different laser pulse parameter (β). The depths of the melt and mushy zones do not change before and after the pulse beginnings of 50th repetitive pulse. However, the radial size of the both zones change during the duration of the 50th pulse. The occurrence of similar depths before and after the pulse heating is because of the absorption of the laser beam along the laser beam axis, which is limited within the liquid zone. This, in turn, increases the melt temperature in the region of the surface. However, in the bottom region of the melt zone as well as in the mushy zone temperature remains the same as the melting temperature of the substrate material. This lowers the temperature gradient in this region, which in turn suppresses the heat diffusion from the melt zone to the mushy zone. Consequently, melting zone size remains the same before and after the heating process due to the 50th pulse. Since the laser power intensity distribution is Gaussian at the surface of the substrate material ($\beta = 0$), laser power reduces with increasing distance in the radial direction from the symmetry axis. This results in relatively shallow melt depth towards the edge of the irradiated spot. Consequently, absorption depth extends towards the solid substrate in this region enhancing the size of the melt and mushy zones in the radial direction during the heating period of the 50th pulse. Moreover, the same arguments are true for $\beta = 0.4$, provided that the sizes of the melt and mushy zones at the end of the 50th heating pulse changes. This is attributed to the shallow melt depth along the laser beam axis. However, as the laser pulse parameter (β) increases further, the melt zone disappears before the initiation of the 50th pulse and melt as well as mushy zones appear after the end of 50th pulse heating period. This is associated with the peak power intensity of the laser pulse. It should be noted that the pulse energy is kept the same for all pulse parameters (β) and increasing (β) lowers the laser peak intensity in the pulse (Fig. 1). Consequently, solid heating and small depth melting are observed in the surface region. Moreover, the location of melting zone changes and moves away from the

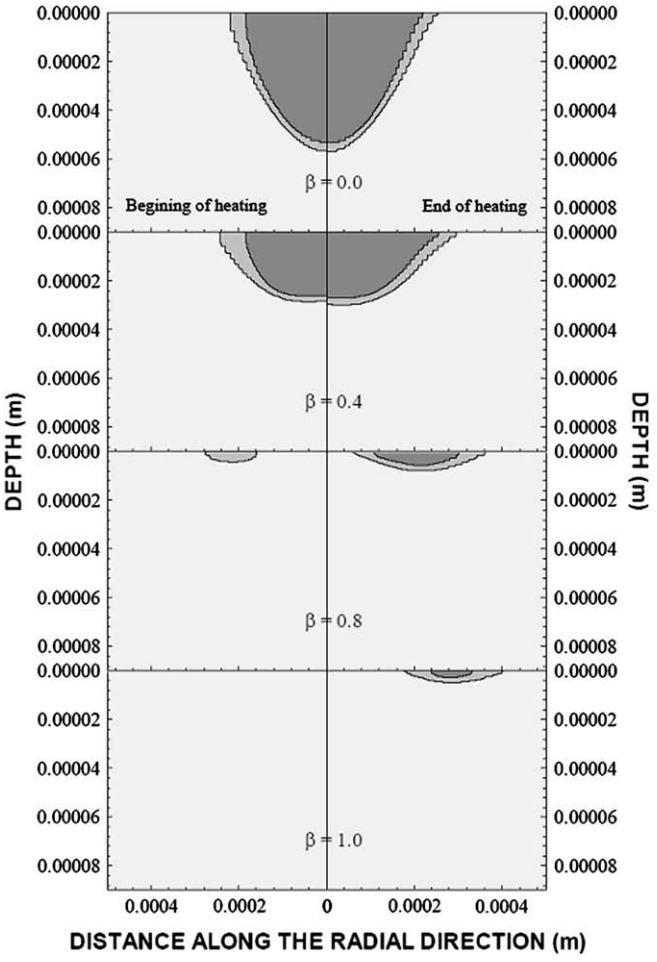

Fig. 5. Liquid and mushy zones inside the substrate material for different β and for the time corresponding to the end of 50th pulse.

symmetry axis in the radial direction. This occurs because of the laser peak power intensity, which is located away from the symmetry axis (Fig. 4).

Fig. 6 shows temporal variation of the surface temperature at the irradiated spot center for different laser pulse parameter (β).

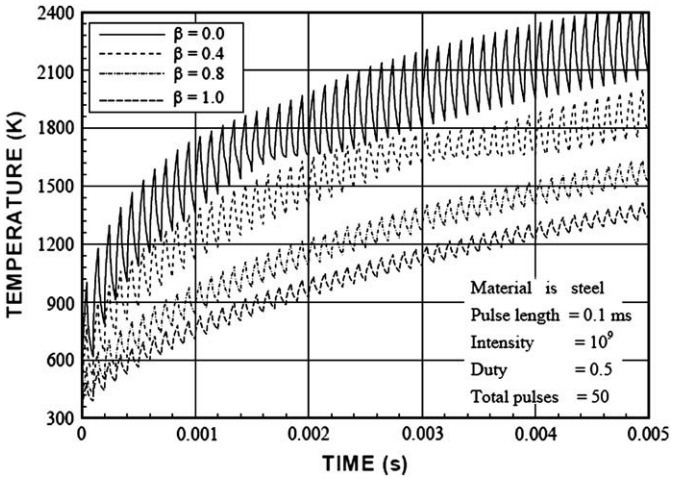

Fig. 6. Temporal variation of surface temperature for different β values. The location is center of irradiated spot.

The spiky appearance of temperature is due to the consecutive pulses, i.e. temperature increases sharply during the heating period of each consecutive pulse and it reduces sharply during the cooling period between two consecutive pulses. Temperature increase is faster in the early heating period and it becomes gradual as the consecutive pulses progresses. The rapid rise of temperature during the early repetition of the consecutive pulses is because of the internal energy gain of the substrate material in the irradiated region during the early heating period. In this case, internal energy gain from the irradiated field in the surface region dominates over the convective and conductive losses from the surface region. This, in turn, enhances temperature rise in this region. Once the consecutive pulses progressed further, the temperature gradient increases in the surface region causing the diffusional energy transfer from this region to the solid bulk. In addition, progressing consecutive pulses result in increased losses from the surface due to attainment of high temperature at the surface. Therefore, conduction and convection losses from the surface region lower the amount of internal energy gain from the irradiated field in the surface region. This suppresses the rate of temperature rise in the surface region. Moreover, once the melting initiates, the amplitude of temperature oscillation reduces as well as the mean temperature, which remains almost the same during the phase change process. In this case, internal energy gain from the irradiated field is partially converted to the latent heat of fusion in the surface region during the melting process. Since the latent heat of fusion is high (Table 1), this suppresses temperature rise in this region. On the other hand, increasing the laser pulse parameter (β) lowers the amplitude of temperature oscillation. This situation is related to laser peak power intensity, which reduces with increasing β. Increasing the laser pulse parameter (β) further, solid heating becomes almost dominant and small size melting in the surface vicinity is observed.

Fig. 7 shows temperature distribution inside the substrate material along the symmetry axis for different laser pulse parameter (β) at the end of the 50th consecutive pulse. Temperature decays sharply from surface towards the solid bulk, which is more pronounced for the laser pulse parameter $\beta = 1$. Moreover, temperature decay becomes gradual as the distance from the surface increases towards the solid bulk. In this case, diffusional energy transport from the surface region to the solid bulk becomes the dominant energy transfer mechanism in this region, i.e., this region extends below the absorption depth. The constant temperature rise due to the melting process is not visible in the figure. This

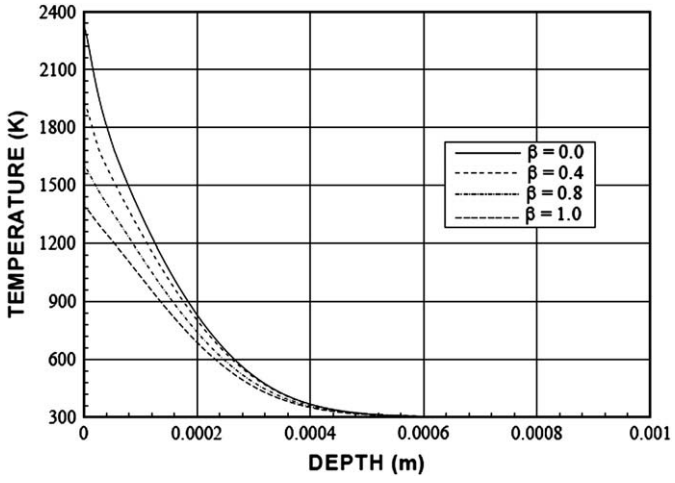

Fig. 7. Temperature distribution along the symmetry axis inside the substrate material for different β values at the end of 50th pulse.

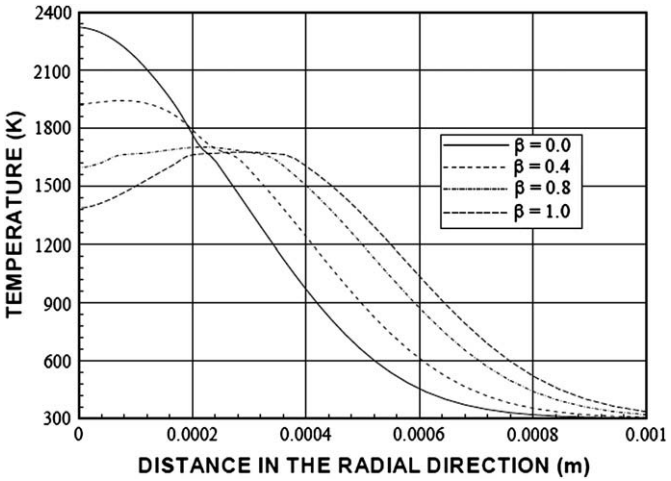

Fig. 8. Temperature distribution along the radial direction at the surface for different β values at the end of 50th pulse.

reveals that melting process is rapid and smooth transition of temperature occurs across the melt–mushy–solid zones. It should be noted that energy content in each pulse with different pulse parameters is kept the same in the simulations. Consequently, temperature decay in the vicinity of the surface changes significantly with the laser pulse parameter despite the fact that all the pulses with different β values have the same energy content.

Fig. 8 shows temperature variation at the surface in the radial direction for different laser pulse parameters at the end of the 50th consecutive pulse. Temperature remains high in the region of the symmetry axis, which is more pronounced for the Gaussian distribution of the pulse intensity ($\beta = 0$). However, as the radial distance increases away from the irradiated spot center, temperature decreases for $\beta \geq 0.4$ while the opposite is true for $\beta < 0.4$. In this case, the attainment of low temperature at the spot center and increasing temperature in the radial direction around the symmetry axis is attributed to the location of laser peak power intensity, which moves away from the symmetry axis with increasing the laser pulse parameter β. The constant temperature region in the temperature profiles is evident for almost all the β values. However, the size of constant temperature region reduces with reducing β. The constant temperature line represents the size of the mushy zone next to the melting zone at the free surface of the substrate material. Consequently, the energy absorbed as well as the amount of heat diffusion in the radial direction is modified by the laser intensity distribution and the location of the corresponding peak intensity at the surface.

5. Conclusion

Laser consecutive pulse heating and melting in the irradiated region of steel is investigated. The influence of laser pulse parameter (β) on temperature distribution as well as melting and mushy zone sizes is examined. Temperature field is computed by using the control volume approach. It is found that high temperature field in the irradiated region results in the formation of the melting and mushy zones in this region, which is particularly true for the Gaussian laser intensity distribution ($\beta = 0$). However, increasing the laser pulse parameter (β) reduces and relocates the laser peak power intensity at the irradiated surface. This, in turn, alters temperature field in the surface region and changes the melting and mushy zone sizes. Moreover, temporal variation of temperature appears in spiky form due to repetitive pulse heating. However, the melting and mushy zones along the symmetry axis

are not affected significantly by the last repetitive pulse (50th pulse), since the depth of melting and mushy zones remains almost the same at the pulse beginning and the pulse ending. This is attributed to the temperature gradient developed in this region, which remains the same before and after the pulse irradiation. This suppresses the conduction heat transfer from the melting zone to mushy zone as well as from mushy zone to solid phase of the substrate material. It should be noted that the rise of the laser intensity at the pulse beginning and the fall of the laser intensity at the pulse ending are not the same. In addition, the consecutive pulse begins after the cooling period of the pervious pulse due to the duty cycle, which in turn, reduces temperature at the pulse beginning. Temperature rise in the early heating period is rapid while it becomes gradual as the consecutive pulses progress. This is associated with the internal energy gain from the irradiated field and conduction as well as convection losses from the surface region. In this case, internal energy gain becomes high in the early heating period promoting temperature rise during this period. Moreover, temperature oscillation at the surface due to repetitive pulses is suppressed during the melting process, which is associated with the latent heat of fusion. The radial distribution of temperature at the surface reveals that mushy zone size increases significantly with increasing the laser pulse parameter (β).

Acknowledgements

The authors acknowledge the support of King Fahd University of Petroleum and Minerals Dhahran Saudi Arabia.

References

[1] J. Zhou, H.L. Tsai, T.F. Lehnhoff, Investigation of transport phenomena and defect formation in pulsed laser keyhole welding of zinc-coated steels, J. Phys. D: Appl. Phys. 39 (2006) 5338–5355.
[2] S. Safdar, L. Li, M.A. Sheikh, Numerical analysis of the effects of non-conventional laser beam geometries during laser melting of metallic materials, J. Phys. D Appl. Phys. 40 (2007) 593–603.
[3] J. Zhou, H.L. Tsai, P.C. Wang, Transport phenomena and keyhole dynamics during pulsed laser welding, Trans. ASME J. Heat Transfer 128 (7) (2006) 680–690.
[4] B.T. Wong, M.P. Menguc, R.R. Vallance, Nano-scale machining via electron beam and laser processing, Trans. ASME J. Heat Transfer 126 (2004) 566–576.
[5] P.M. Raj, S. Sarkar, S. Chakraborty, P. Dutta, Three-dimensional computational modeling of momentum, heat and mass transfer in laser surface alloying with distributed melting of alloying element, Int. J. Numer. Methods Heat Fluid Flow II (6) (2001) 576–599.
[6] A. Fathi, E. Toyserkani, A. Khajepour, M. Durali, Prediction of melt pool depth and dilution in laser powder deposition, J. Phys. D Appl. Phys. 39 (2006) 2613–2623.
[7] Z.H. Shen, S.Y. Zhang, J. Lu, X.W. Ni, Mathematical modeling of laser induced heating and melting in solids, Opt. Laser Technol. 33 (2001) 533–537.
[8] J.D. Van de Ven, A.G. Erdman, Laser transmission welding of thermoplastics – part I: temperature and pressure modeling, Trans. ASME J. Mat. Sci. Eng. 129 (2007) 849–857.
[9] D. Chatterjee, S. Chakraborty, An enthalpy-based lattice Boltzmann model for diffusion dominated solid–liquid phase transformation, Phys. Lett. A 341 (2005) 320–330.
[10] P.M. Raj, S. Sarkar, S. Chakraborty, P. Dutta, Three-dimensional computational modeling of momentum, heat and mass transfer in a laser surface alloying process, Numer. Heat Transfer A 42 (2002) 307–326.
[11] B.S. Yilbas, S.B. Mansoor, Laser evaporative heating of surface: simulation of flow field in the laser produced cavity, J. Phys. D Appl. Phys. 39 (17) (2006) 3863–3875.
[12] B.S. Yilbas, S. Bin Mansoor, S.Z. Shuja, H. Abualhamayel, Laser pulse heating and vapor front generation, AIChE J. 54 (2008) 627–638.
[13] Amada BP 41040, 95912 Roissy Aeroport Cedex, France.
[14] Fluent Inc, Fluent Users Guide, Fluent Inc, 2005.
[15] B.S. Yilbas, S.Z. Shuja, M.O. Budair, Nano-second pulse heating and gas assisting jet considerations, Int. J. Mach. Tools Manuf. 40 (2000) 1023–1038.
[16] V.R. Voller, C. Prakash, A fixed-grid numerical modeling methodology for convection–diffusion mushy region phase-change problems, Int. J. Heat Mass Transfer 30 (1987) 1709–1720.
[17] S.V. Patankar, Numerical Heat Transfer, McGraw-Hill, New York, 1980.
[18] F.P. Incropera, D.P. DeWitt, Fundamentals of Heat and Mass Transfer, fourth ed. John Wiley & Sons, New York, 1996, pp. 829–830.
[19] K.C. Mills, Thermophysical Properties for Selected Commercial Alloys, Woodhead Publishing Ltd, Cambridge, UK, 2002, pp. 127–205.